Contents lists available at SciVerse ScienceDirect

Journal of Contaminant Hydrology

journal homepage: www.elsevier.com/locate/jconhyd

Colloid transport in dual-permeability media

Feike J. Leij [a,*], Scott A. Bradford [b]

[a] Dept. of Civil Engineering and Construction Engineering Management, California State University, 1250 Bellflower Boulevard – MS5101, VEC-206, Long Beach, CA 90840-5101, USA
[b] US Salinity Laboratory, USDA, ARS, 450W. Big Springs Road, Riverside, CA 92507-4617, USA

ARTICLE INFO

Article history:
Received 13 October 2012
Received in revised form 27 March 2013
Accepted 28 March 2013
Available online 19 April 2013

Keywords:
Analytical solution
Colloid retention
Optimization
Solute transport

ABSTRACT

It has been widely reported that colloids can travel faster and over longer distances in natural structured porous media than in uniform structureless media used in laboratory studies. The presence of preferential pathways for colloids in the subsurface environment is of concern because of the increased risks for disease caused by microorganisms and colloid-associated contaminants. This study presents a model for colloid transport in dual-permeability media that includes reversible and irreversible retention of colloids and first-order exchange between the aqueous phases of the two regions. The model may also be used to describe transport of other reactive solutes in dual-permeability media. Analytical solutions for colloid concentrations in aqueous and solid phases were obtained using Laplace transformation and matrix decomposition. The solutions proved convenient to assess the effect of model parameters on the colloid distribution. The analytical model was used to describe effluent concentrations for a bromide tracer and 3.2- or 1-μm-colloids that were observed after transport through a composite 10-cm long porous medium made up of a cylindrical lens or core of sand and a surrounding matrix with sand of a different grain size. The tracer data were described very well and realistic estimates were obtained for the pore-water velocity in the two flow domains. An accurate description was also achieved for most colloid breakthrough curves. Dispersivity and retention parameters were typically greater for the larger 3.2-μm-colloids while both reversible and irreversible retention rates tended to be higher for the finer sands than the coarser sand. The relatively small sample size and the complex flow pattern in the composite medium made it difficult to reach definitive conclusions regarding transport parameters for colloid transport.

1. Introduction

Many porous media or geological formations consist of regions with different porosity and permeability that can create preferential flow pathways for water and contaminants. Examples of such media are fractured rock, cracked clay soils, agricultural soils containing macropores created by burrowing earthworm and animals, or structured soils with inter- and intra-aggregate pore space. Factors that influence soil formation and management will also create spatial variations in soil hydraulic properties that are ubiquitous in natural environments.

Field experiments frequently indicate that colloids can travel faster and over longer distances than would be expected based on results from laboratory studies in homogeneous porous media because of these types of preferential flow pathways (Beven and Germann, 1982; Cey and Rudolph, 2009; Cey et al., 2009; Dean and Foran, 1992; Evans and Owens, 1972; Jarvis, 2007; McGechan and Lewis, 2002; Pang et al., 2008; Passmore et al., 2010). The preferential transport of colloids is of special concern because of the increased risk of dissemination and exposure of humans and animals to disease causing microorganisms and colloid-associated contaminants (Simunek et al., 2006; Unc and Goss, 2003).

It is extremely difficult, if not impossible, to deterministically model the complexities of preferential flow pathways in natural subsurface environments. Simplified deterministic and

* Corresponding author. Tel.: +1 562 985 5119.
E-mail addresses: Feike.Leij@csulb.edu (F.J. Leij), Scott.Bradford@ars.usda.gov (S.A. Bradford).

0169-7722/$ – see front matter © 2013 Elsevier B.V. All rights reserved.
http://dx.doi.org/10.1016/j.jconhyd.2013.03.010

stochastic models have therefore been developed to simulate the preferential transport of contaminants (Gerke and van Genuchten, 1996; Selim and Ma, 1998; Simunek and van Genuchten, 2008; Toride et al., 1995). In the most widely examined scenario, there is water flow in an inter-aggregate or "mobile" aqueous region and no flow in an intra-aggregate or "immobile" aqueous region (Selim and Ma, 1998). Analytical solutions have been developed for mobile–immobile transport of solutes by assuming linear solute exchange between the mobile and immobile regions (Coats and Smith, 1964; Lapidus and Amundson, 1952; van Genuchten and Wierenga, 1976) or kinetic and linear exchange between the two regions (Leij and Bradford, 2009). For well-defined aggregates it is possible to directly apply Fick's law for diffusive transfer in the immobile region (cf. van Genuchten and Dalton, 1986).

More general dual-permeability models are needed when there is flow in both pore domains to account for many of the complexities that are observed, e.g., multi-peak breakthrough curves (Gerke and van Genuchten, 1996; Simunek and van Genuchten, 2008). Analytical approaches for solute transport with water flow in both domains have received limited attention (e.g., Dykhuizen, 1991; Leij et al., 2012). The utility of analytical solutions for simplified transport models has been pointed out by, among many others, Javandel et al. (1984) and Vanderborght et al. (2005). The emphasis of this study is on the analytical modeling of the fate and transport of colloids in dual-permeability media. It should be mentioned that the dual-permeability modeling approach has also been applied to describe colloid transport in homogeneous media because of the potential for different rates of colloid migration with advection in the bulk aqueous phase and rolling of colloids on the solid phase (Bradford et al., 2009, 2011).

Subsurface transport of colloids has often been modeled in a similar manner as that of generic solutes, but additional complexities are to be expected. For example, colloid retention in homogeneous soils is dependent on attachment and straining processes that are sensitive to the system hydrodynamics, the input colloid concentration, the colloid size, the soil type and texture, the solution and solid phase chemistry, and the water content (Bradford and Torkzaban, 2008; Ryan and Elimelech, 1996). These retention processes may be reversible or irreversible depending on the nature and location of the interaction. Colloids experience strong, largely irreversible interactions in a primary minimum when there is no energy barrier to attachment (favorable conditions). Conversely, the interactions are much weaker and reversible when colloids are associated with a secondary minimum under unfavorable (in the presence of an energy barrier) attachment conditions. In this case, enhanced colloid retention has been observed in locations associated with weaker hydrodynamic forces (grain–grain contacts and larger surface roughness locations) or enhanced adhesive forces (chemical heterogeneity arising from metal oxides, adsorbed divalent cations, and clays) (Bradford and Torkzaban, 2008).

It is hence clear that models for colloid transport will be more complex and approximate than models for solute transport. Application of a dual-permeability model that allows for both reversible and irreversible colloid retention processes is believed to partly deal with the added complexity. There will be some error in lumping reversible attachment and depth-dependent straining (Bradford et al., 2003, 2011) that is sensitive to the presence of textural interfaces (Bradford et al., 2005; Silliman, 1995) into effective dual-permeability model parameters. Furthermore, the exchange of colloids between the two flow domains is expected to be a function of the amount of colloid retention in each region and there may be size exclusion in finer textured media (Bradford et al., 2003; Ginn et al., 2002; Ryan and Elimelech, 1996).

The objective of this work is to provide an analytical solution for colloid transport in dual-permeability media for a model that includes reversible and irreversible retention of colloids and first-order exchange between the aqueous phases of the two regions. The analytical solution can also be applied to transport of other reactive solutes in porous media. The analytical solution will be applied to colloid displacement experiments reported by Bradford et al. (2004) involving a medium made up of a cylindrical volume of soil embedded in a different soil packed in a hollow aluminum cylinder. Due to

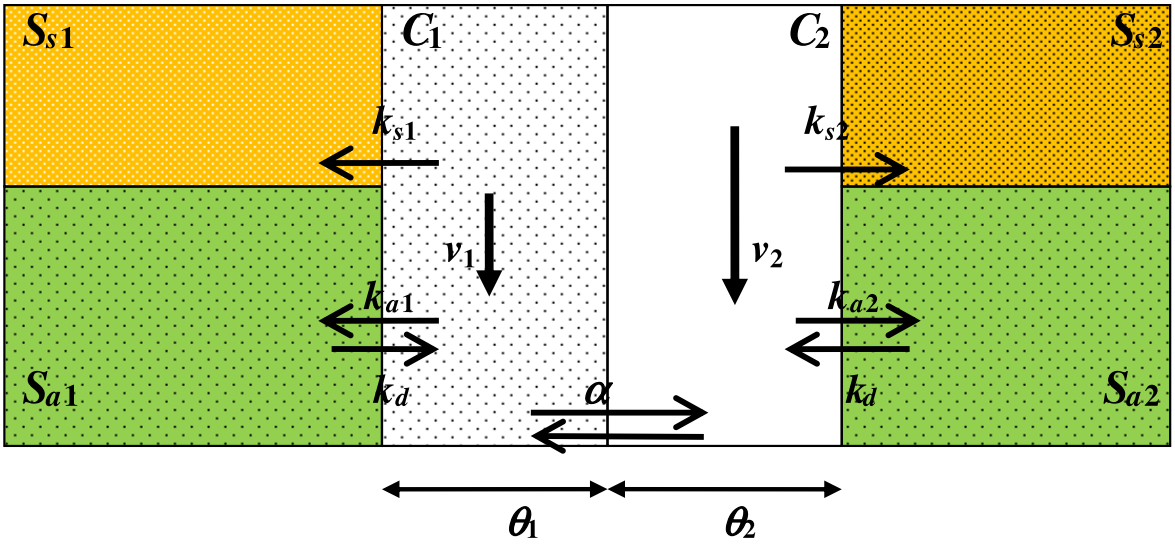

Fig. 1. Schematic of dual-velocity model for colloid transport.

differences in permeability and other soil properties, the colloids were transported at a substantially different rate in the two soil materials with rate-limited exchange between them and the composite soil may be viewed as a dual-permeability medium. Simultaneously observed transport of a bromide tracer was modeled by modifying the solution by Leij et al. (2012) for transport of generic solutes in dual-permeability media according to the dual-advection dispersion equation (DADE).

2. Mathematical problem and solution

The following transport mechanisms are considered: advection, dispersion, and exchange between the liquid phase of the low- and high-permeability regions 1 and 2. Two kinetic retention sites are available for each region. Fig. 1 provides a schematic outline of the various processes and the notation that will be employed. The general equation for transport in region i with linear exchange to region j is given by:

$$\rho\frac{\partial S_{ai}}{\partial t}+\rho\frac{\partial S_{si}}{\partial t}+\theta_i\frac{\partial C_i}{\partial t}=\theta_i D_i\frac{\partial^2 C_i}{\partial x^2}-\theta_i v_i\frac{\partial C_i}{\partial x}+\alpha\left(C_j-C_i\right) \quad (1)$$

$(i=1,2;j=2,1)$

where t is time [T], x is distance [L], D_i is longitudinal dispersion coefficient [L^2/T], v_i is pore-water velocity [L/T] — where it is arbitrarily assumed that $v_1 < v_2$, C_i is the liquid phase concentration expressed as number of colloids per aqueous volume of region i [$N_c\ L^{-3}$], S_{ai} and S_{si} are the solid phase concentrations for reversibly and irreversibly retained colloids, respectively, expressed as number of colloids originating from aqueous region i per mass of bulk soil [$N_c\ M^{-1}$], θ_i is the volumetric water content in terms of volume of water in region i per bulk volume [$L^3_{w,i}\ L^{-3}$], ρ is the soil bulk density assumed to be equal for both soils and given as mass of bulk soil per bulk volume [ML^{-3}], and α is the coefficient for mass transfer between the two aqueous regions [T^{-1}]. One kinetic retention site employs a conventional attachment and detachment model to describe behavior of reversibly retained colloids to and from the aqueous and solid phases as:

$$\rho\frac{\partial S_{ai}}{\partial t}=\theta_i k_{ai}C_i-\rho k_d S_{ai} \quad (i=1,2) \quad (2)$$

where k_{ai} is the coefficient for attachment of colloids from aqueous region i onto the solid phase [T^{-1}] and k_d is the coefficient for detachment of colloids from the solid into the aqueous phase [T^{-1}]. The second kinetic site considers irreversible colloid retention due to straining or attachment in a primary minimum as:

$$\rho\frac{\partial S_{si}}{\partial t}=\theta_i k_{si}C_i \quad (i=1,2) \quad (3)$$

with k_{si} as the coefficient for irreversible colloid retention from the aqueous region i onto the solid phase [T^{-1}]. It should be mentioned that the irreversible retention site may also be employed to account for processes such as inactivation or degradation.

The problem is solved for the case where the medium is initially free of colloids and a step pulse of magnitude C_o is applied to the inlet with a zero-gradient concentration at a fictitious outlet at infinity. The corresponding conditions are:

$$C_i-\delta\kappa_i\frac{\partial C_i}{\partial x}=C_o \qquad \delta=\begin{cases}0 & \text{first type}\\ 1 & \text{third type}\end{cases} \quad (4)$$

$$C_i(x,0)=0 \quad (5)$$

$$\frac{\partial C_i}{\partial x}(\infty,t)=0 \quad (6)$$

where C_o is the concentration of the applied solution and δ is used to allow the inlet condition to be applicable to either a first- or third-type inlet condition, which respectively corresponds to a flux- or volume-averaged detection mode. A zero-gradient outlet condition is assumed at an infinite distance.

The dispersion coefficient is written as

$$D_i=\kappa v_i \quad (7)$$

with κ as dispersivity (L). The solution of the governing equations is outlined in Appendix A. The solution may be written as:

$$\begin{aligned}C_1(x,t)=&\int_{\frac{a_1 t}{a_1+a_2}}^{t}F(\tau)\Bigg\{\exp\left(-\frac{d_1\tau}{a_1}\right)J_0(\omega\phi_0)\\&+\exp\left(-\frac{\tau-\eta_1}{a_1/d_1}+\frac{\gamma_1}{k_d},k_d\eta_1\right)+\\&+\int_0^{\tau_1}\exp\left(-\frac{\tau-\eta}{a_1/d_1}-k_d\eta\right)\sqrt{\frac{\overline{\gamma}}{\eta}}I_1(2\sqrt{\gamma\eta})J_0(\omega\phi)\\&-\exp\left(-\frac{\tau-\eta}{a_1/d_1}+\frac{\gamma}{k_d}\right)\Bigg[J\left(\frac{\gamma}{k_d},k_d\eta\right)\frac{\omega(t-\tau)}{a_2/a_1}\frac{J_1(\omega\phi)}{\phi}\\&+\left(\frac{b_1}{a_1k_d}\left[1-J\left(k_d\eta,\frac{\gamma}{k_d}\right)\right]-\frac{d_4}{a_1}J\left(\frac{\gamma}{k_d},k_d\eta\right)\right)J_0(\omega\phi)]d\eta\Bigg\}d\tau\\&-\int_{\frac{a_1 t}{a_2-a_1}}^{t}F(\tau)\Bigg\{\exp\left(-\frac{d_1\tau}{a_1}\right)J_0(\omega\phi_0)\\&-\exp\left(-\frac{\tau-\eta_2}{a_1/d_1}+\frac{\gamma_2}{k_d}\right)J\left(\frac{\gamma_2}{k_d},k_d\eta_2\right)+\\&+\int_0^{\tau_2}\exp\left(-\frac{\tau-\eta}{a_1/d_1}-k_d\eta\right)\sqrt{\frac{\overline{\gamma}}{\eta}}I_1(2\sqrt{\gamma\eta})J_0(\omega\phi)\\&-\exp\left(-\frac{\tau-\eta}{a_1/d_1}+\frac{\gamma}{k_d}\right)\Bigg[J\left(\frac{\gamma}{k_d},k_d\eta\right)\frac{\omega(t-\tau)}{a_2/a_1}\frac{J_1(\omega\phi)}{\phi}\\&+\left(\frac{b_1}{a_1k_d}\left[1-J\left(k_d\eta,\frac{\gamma}{k_d}\right)\right]-\frac{d_4}{a_1}J\left(\frac{\gamma}{k_d},k_d\eta\right)\right)J_0(\omega\phi)]d\eta\Bigg\}d\tau\end{aligned} \quad (8)$$

$$C_2(x,t) = \int_{-\frac{a_1 t}{a_2+a_1}}^{t} F(\tau)\Bigg\{ \exp\left(-\frac{d_1\tau}{a_1}\right) J_0(\omega\phi_0) + \exp\left(-\frac{\tau-\eta_2}{a_1/d_1}+\frac{\gamma_2}{k_d}\right) J\left(\frac{\gamma_2}{k_d}, k_d\eta_2\right) + \int_0^{\tau_2} \exp\left(-\frac{\tau-\eta}{a_1/d_1}-k_d\eta\right)\sqrt{\frac{\gamma}{\eta}} I_1(2\sqrt{\gamma\eta}) J_0(\omega\phi) + \exp\left(-\frac{\tau-\eta}{a_1/d_1}+\frac{\gamma}{k_d}\right)\Bigg[J\left(\frac{\gamma}{k_d}, k_d\eta\right)\frac{\omega(t-\tau)}{a_2/a_1}\frac{J_1(\omega\phi)}{\phi} - \left(\frac{b_1}{a_1 k_d}\left[1-J\left(k_d\eta, \frac{\gamma}{k_d}\right)\right] - \frac{d_3}{a_1} J\left(\frac{\gamma}{k_d}, k_d\eta\right)\right) J_0(\omega\phi)\Bigg] d\eta \Bigg\} d\tau - \int_{\frac{a_1 t}{a_1+a_2}}^{t} F(\tau)\Bigg\{ \exp\left(-\frac{d_1\tau}{a_1}\right) J_0(\omega\phi_0) + \exp\left(-\frac{\tau-\eta_1}{a_1/d_1}+\frac{\gamma_1}{k_d}\right) J\left(\frac{\gamma_1}{k_d}, k_d\eta_1\right) + \int_0^{\tau_1} \exp\left(-\frac{\tau-\eta}{a_1/d_1}-k_d\eta\right)\sqrt{\frac{\gamma}{\eta}} I_1(2\sqrt{\gamma\eta}) J_0(\omega\phi) + \exp\left(-\frac{\tau-\eta}{a_1/d_1}+\frac{\gamma}{k_d}\right)\Bigg[J\left(\frac{\gamma}{k_d}, k_d\eta\right)\frac{\omega(t-\tau)}{a_2/a_1}\frac{J_1(\omega\phi)}{\phi} - \left(\frac{b_1}{a_1 k_d}\left[1-J\left(k_d\eta, \frac{\gamma}{k_d}\right)\right] - \frac{d_3}{a_1} J\left(\frac{\gamma}{k_d}, k_d\eta\right)\right) J_0(\omega\phi)\Bigg] d\eta \Bigg\} d\tau. \quad (9)$$

For a first-type inlet condition (flux-averaged concentration)

$$F(\tau) = \frac{C_o}{2}\frac{x}{\sqrt{8\pi v_1 v_2 \kappa (t-\tau)^3/a_2}} \exp\left(-\frac{[a_2 x - 2v_1 v_2 (t-\tau)]^2}{8 a_2 v_1 v_2 \kappa (t-\tau)} - \frac{d_2}{a_2}(t-\tau)\right) \quad (10a)$$

while for a third-type condition (volume-averaged concentration):

$$F(\tau) = \frac{C_o}{2}\exp\left[-\frac{d_2}{a_2}(t-\tau)\right] \times \Bigg\{ \sqrt{\frac{2v_1 v_2}{\pi a_2 \kappa (t-\tau)}} \exp\left(-\frac{[a_2 x - 2v_1 v_2 (t-\tau)]^2}{8 a_2 v_1 v_2 \kappa (t-\tau)}\right) - \frac{v_1 v_2}{a_2 \kappa}\exp\left(\frac{x}{\kappa}\right)\operatorname{erfc}\left(\frac{a_2 x + 2 v_1 v_2 (t-\tau)}{\sqrt{8 a_2 v_1 v_2 \kappa (t-\tau)}}\right)\Bigg\} \quad (10b)$$

The following auxiliary variables are used in the expressions for the two concentrations:

$$a_1 = v_2 - v_1, \quad a_2 = v_2 + v_1 \quad (11a, b)$$

$$b_1 = (k_{a1} v_2 - k_{a2} v_1) k_d \quad , \quad b_2 = (k_{a1} v_2 + k_{a2} v_1) k_d \quad (12a, b)$$

$$d_1 = (k_{a1} + k_{s1} + \alpha_1) v_2 - (k_{a2} + k_{s2} + \alpha_2) v_1 \quad , \quad d_2 = (k_{a1} + k_{s1} + \alpha_1) v_2 + (k_{a2} + k_{s2} + \alpha_2) v_1 \quad (13a, b)$$

$$d_3 = (k_{a1} + k_{s1} + \alpha_1) v_2 - (k_{a2} + k_{s2} - \alpha_2) v_1 \quad , \quad d_4 = (k_{a1} + k_{s1} - \alpha_1) v_2 - (k_{a2} + k_{s2} + \alpha_2) v_1 \quad (14a, b)$$

and

$$\omega = \frac{2}{a_1}\sqrt{\alpha_1 v_1 \alpha_2 v_2} \quad , \quad \alpha_i = \alpha/\theta_i. \quad (15a, b)$$

Dummy temporal variables are as follows:

$$\gamma = \frac{t-\tau}{a_2/b_2} + \frac{\tau-\eta}{a_1/b_1} \quad , \quad \gamma_1 = \frac{t-\tau}{a_2/b_2} + \frac{\tau-\tau_1}{a_1/b_1} \quad , \quad \gamma_2 = \frac{t-\tau}{a_2/b_2} + \frac{\tau-\tau_2}{a_1/b_1} \quad (16a, b, c)$$

with

$$\tau_1 = \tau - \frac{t-\tau}{a_2/a_1} \quad , \quad \tau_2 = \tau + \frac{t-\tau}{a_2/a_1} \quad (17a, b)$$

and

$$\phi = \sqrt{(\tau-\eta)^2 - \left(\frac{t-\tau}{a_2/a_1}\right)^2} \quad , \quad \phi_0 = \sqrt{\tau^2 - \left(\frac{t-\tau}{a_2/a_1}\right)^2}. \quad (18a, b)$$

Furthermore, J_0 and J_1 are zero- and first-order Bessel functions of the first kind, I_0 and I_1 are the corresponding modified Bessel functions, and J denotes Goldstein's J-function (cf. Goldstein, 1953; van Genuchten, 1981).

The solid phase concentration for reversible and irreversibly retained colloids in domain i, S_{ai} and S_{si}, are expressed as number of colloids per mass of bulk soil. They are obtained from the aqueous concentrations according to:

$$S_{ai} = \frac{k_{ai}\theta_i}{\rho}\int_0^t \exp[-k_d(t-\tau)] C_i(z,\tau) d\tau \quad (19)$$

$$S_{si} = \frac{k_{si}\theta_i}{\rho}\int_0^t C_i(z,\tau) d\tau. \quad (20)$$

The effluent concentration of a colloid or tracer is defined as the ratio of the advective solute flux and the water flux for both domains or as the sum of individual effluent concentrations:

$$C_e = C_{e1} + C_{e2} \quad , \quad C_{ei} = \theta_i v_i C_i / \theta v. \quad (21)$$

The total colloid concentration in the soil, given as number of colloids per mass of soil, is given by:

$$C_T = (\theta_1 C_1 + \theta_2 C_2)/\rho + S_{a1} + S_{s1} + S_{a2} + S_{s2}. \quad (22)$$

The integrals in the analytical solutions were evaluated using 100-point Gauss–Chebyshev quadrature. The results of the analytical solution were compared to those obtained by numerically inverting the Laplace transform according to de Hoog et al. (1982). Fig. 2 contains effluent curves predicted analytically and numerically for a pulse application of colloids subject to two different transfer parameters, reversible attachment, and no irreversible retention. There is a close correspondence between the analytical and the numerical results.

3. Sensitivity analysis

The analytical solutions presented in the previous section are convenient to illustrate the sensitivity of colloid concentration, as a function of time or position, to the various transport and retention parameters. The effect of the transfer

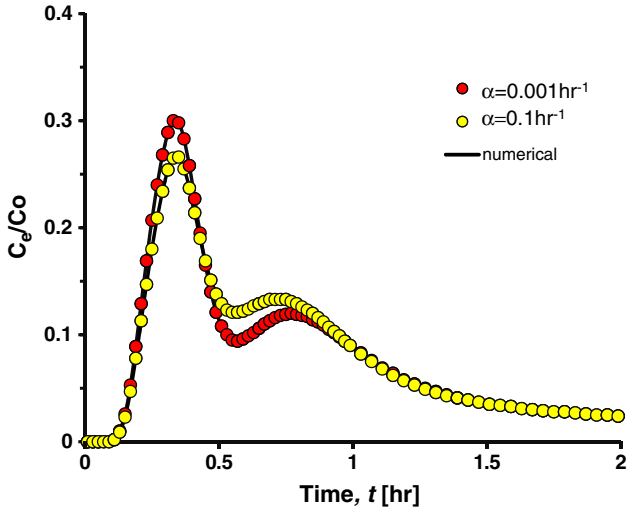

Fig. 2. Numerical and analytical solutions for effluent curves at $x = 10$ cm as result of a pulse input ($t_o = 0.2$ h) with $v_1 = 12.5$ cm/h, $\theta_1 = 0.4$, $v_2 = 40$ cm/h, $\theta_2 = 0.1$, dispersivity $\kappa = 0.5$ cm, reaction rates $k_{a1} = k_{a2} = 1$ h^{-1}, $k_{s1} = k_{s2} = 0$, and $k_d = 1$ h^{-1}, and transfer parameter $\alpha = 0.001$ or 0.1 h^{-1}.

parameter α is illustrated in Fig. 3 for a nonreactive solute such as the bromide. Values of C_e are normalized by the input concentration (C_o). A solute was applied for a period of $t_o = 0.2$ h and the effluent concentration was predicted as a function of time at a distance of 10 cm using the solutions in Section 2 for a step input (cf. Toride et al. 1993). The contribution of slower and more prevalent domain 1 ($v_1 = 12.5$ cm/h, $\theta_1 = 0.4$) and domain 2 ($v_2 = 100$ cm/h, $\theta_2 = 0.1$) are depicted in Fig. 3 for the three transfer rates of $\alpha = 0.001$, 0.1, and 10 h^{-1}. At the relatively low value for α of 0.001 h^{-1} there is very little solute transfer between the two domains. The overall effluent curve has two distinct peaks with early breakthrough for domain 2 and later breakthrough for domain 1. There is more solute exchange at the intermediate value of 0.1 h^{-1} with earlier breakthrough in domain 1, due to solute that resided originally in domain 2, and tailing in domain 2, which is caused by solute that moved from domain 1 to 2. The overall breakthrough curve still has two distinct peaks. Finally, for $\alpha = 10$ h^{-1} transport is essentially an "equilibrium" process with rapid exchange between the two flow domains to counteract any difference in concentration. Hence the breakthrough curve has a single peak and is formed by superposition of two very similar curves for domains 1 and 2.

Reversible retention of colloids is illustrated in Fig. 4. The colloid is subject to attachment at a rate of 10 h^{-1} for both domains. Irreversibly colloid retention was not considered in this scenario. Colloids profiles in a 50-cm long soil show the contribution of the aqueous and solid phase to the total concentration. For a relatively low detachment rate $k_d = 1$ h^{-1}, virtually all the colloid is attached with little remaining in (or returning to) the aqueous phase. There is virtually no bimodal behavior of the colloid profiles. For the higher detachment rate of 10 h^{-1}, appreciable amounts of colloids can be found in both the aqueous and the solid phases. Furthermore, the colloid profiles exhibits bimodality. Notice that for the faster region 2 the amount of colloid in the solid phase of the first 5 cm greatly exceeds the amount in the aqueous phase, the latter was mostly subjected to an attachment-detachment sequence. For a high k_d of 100 h^{-1} colloid will not remain attached for considerable

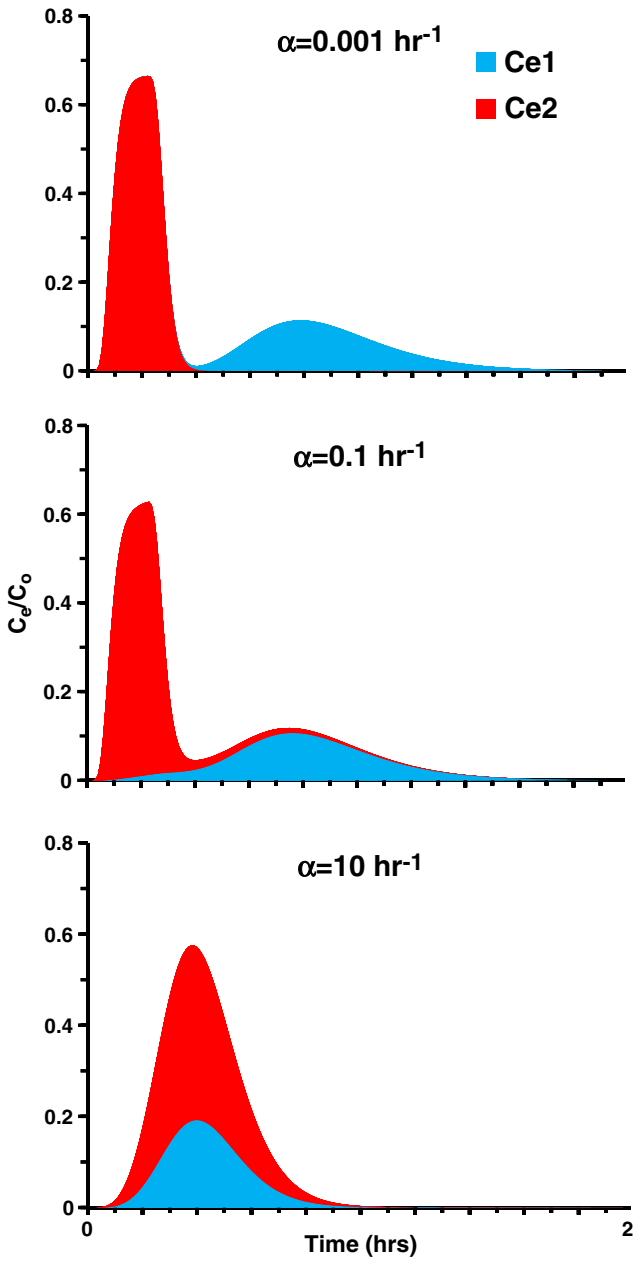

Fig. 3. Effluent curves for a nonreactive solute at $x = 10$ cm as result of a pulse input ($t_o = 0.2$ h) with $v_1 = 12.5$ cm/h, $\theta_1 = 0.4$, $v_2 = 100$ cm/h, $\theta_2 = 0.1$, dispersivity $\kappa = 0.5$ cm, and transfer parameter $\alpha = 0.001$, 0.1, or 10 h^{-1}.

time and the amount of colloid in the solid phase is minuscule compared to the aqueous phase. The total colloid concentration profile shows strong bimodal behavior with peaks at approximately 5 and 25 cm.

Finally, the effect of irreversible colloid retention is illustrated in Fig. 5. Profiles of reversibly and irreversibly retained colloids are shown as a function of distance for domains 1 and 2. Three different values of $k_{s1} = k_{s2}$ were used (viz. 1, 2, and 4 h^{-1}) whereas the attachment and detachment rates were 5 and 10 h^{-1}, respectively, in both domains. As expected, the solid phase concentrations of irreversibly retained colloids rapidly decrease with distance. For the lower $k_{s1} = k_{s2} = 1$ h^{-1}, the total colloid profile exhibits a bimodal distribution with a substantial part of the colloid in the aqueous

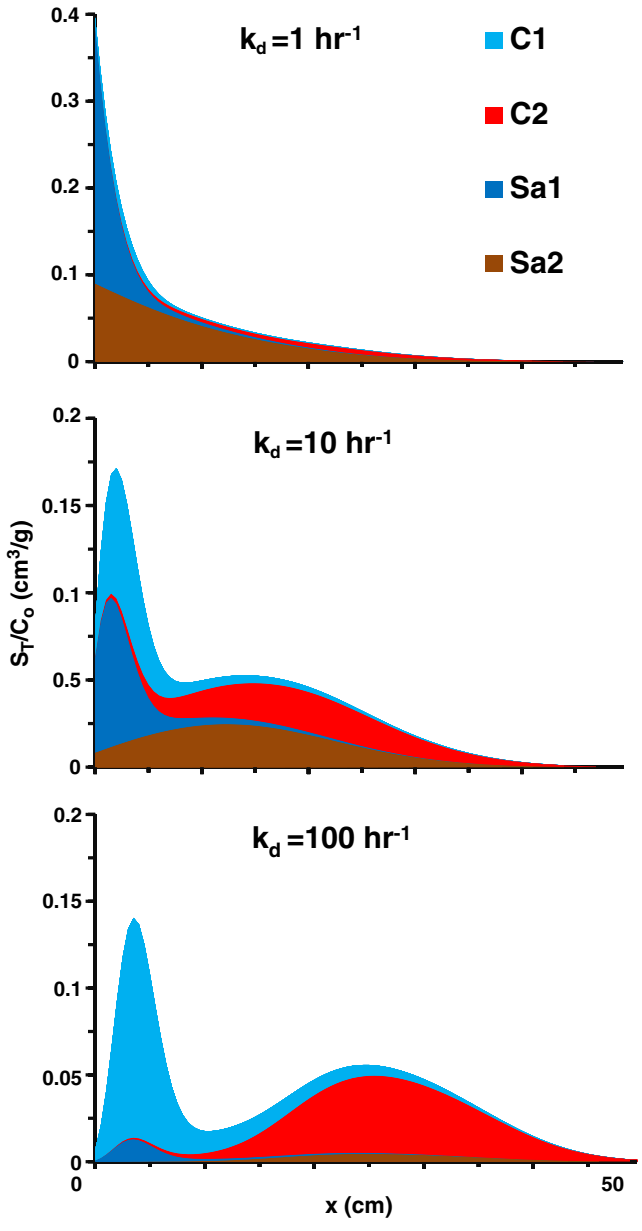

Fig. 4. Solute profiles for a reactive solute at $t = 0.4$ h as result of a pulse input ($t_o = 0.2$ h) with $v_1 = 12.5$ cm/h, $\theta_1 = 0.4$, $v_2 = 100$ cm/h, $\theta_2 = 0.1$, dispersivity $\kappa = 0.5$ cm, transfer parameter $\alpha = 0.1$ h^{-1}, and reaction rates $k_{a1} = k_{a2} = 10$ h^{-1}, $k_{s1} = k_{s2} = 0$, and $k_d = 1$, 10, or 100 h^{-1}.

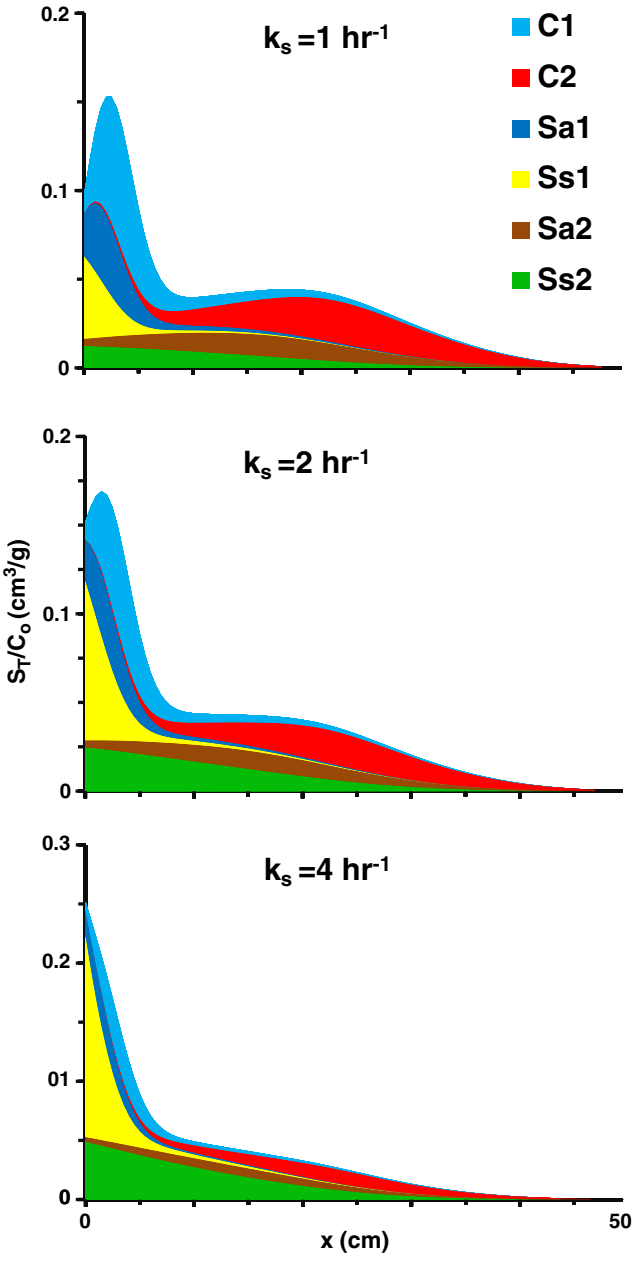

Fig. 5. Solute profiles for a reactive solute at $t = 0.4$ h as result of a pulse input ($t_o = 0.2$ h) with $v_1 = 12.5$ cm/h, $\theta_1 = 0.4$, $v_2 = 100$ cm/h, $\theta_2 = 0.1$, dispersivity $\kappa = 0.5$ cm, transfer parameter $\alpha = 0.1$ h^{-1}, and reaction rates $k_{a1} = k_{a2} = 5$ h^{-1}, $k_d = 10$ h^{-1}, and $k_{s1} = k_{s2} = 1$, 2, or 4 h^{-1}.

phase or attached to the solid phase. Increasing k_{s1} and k_{s2} to 2 h^{-1} and, especially, 4 h^{-1} results in an increased amount of irreversibly retained colloids, which can no longer appear in the aqueous or attached phases.

4. Experimental and data optimization

4.1. Experimental procedure

Bradford et al. (2004) used 10-cm-long, 5-cm-diameter aluminum columns that were macroscopically nonuniform as illustrated in Fig. 6 and consisted of different Ottawa sands, which will be identified by their median grain size of 710, 360, 240, and 150 μm. The interior of the medium is formed by a 6-cm-long, 2.3-cm-diameter sand column — referred to as the lens. The remainder of the space of the aluminum core was filled with sand with a different median grain size — referred to as the matrix. During steady-state, upward flow through the vertical column, a 1.33-h pulse of 0.001 *M* NaBr and 1-μm- or 3.2-μm-diameter colloids (microspheres with a carboxyl surface) was applied to the soil column. Approximately 50 effluent samples were collected over a period of four hours during displacement experiments to determine bromide and colloid concentrations versus time.

Because the permeability of the lens and the matrix will be different, water flow will not be uniform. Based on numerical simulations by Bradford et al. (2004), the flow appears to be approximately one-dimensional in a substantial part of the column and transport in the column may be described by the dual-permeability model. The porosity and the Darcy flux for

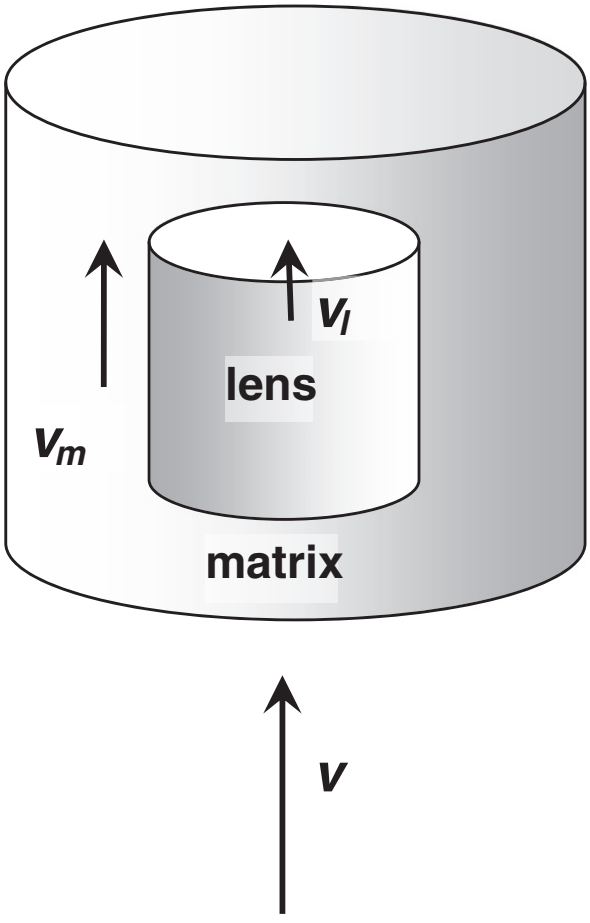

Fig. 6. Schematic of composite medium with a lens and matrix of different soil material.

the heterogeneous (composite) medium were determined from the overall bulk density, assuming a specific solid density of 2.65 g/cm^3, and the volumetric flow rate of the effluent, respectively. A total of twelve experiments were conducted with the 710-μm Ottawa sand being the matrix (sleeve) for the first six and the lens (center) for the last six experiments. Table 1 lists the median particle diameter, d_{sand}, for matrix and lens, the colloid size, $d_{colloid}$, the overall volumetric water content, θ, and the Darcy flux, q, for each experiment. Also presented is the recovered fraction of colloids, which is determined from the total number of colloids detected in the effluent samples relative to the total number applied.

4.2. Bromide effluent curves

Breakthrough data for the nonreactive bromide tracer were described by using the analytical solution for the DADE (Leij et al., 2012) with a data optimization routine based upon the CXTFIT program (Toride et al., 1995). There are many potential optimization parameters. Two velocities, one volumetric water content, transfer parameter, α, dispersivity, κ, and pulse duration, t_o, were optimized in this study. Some of the optimized parameters for the bromide displacement were later used as input in the model for colloid transport. Table 2 lists pertinent parameters along with the coefficient of determination r^2 for the description of the bromide effluent curves for the twelve experiments. The pore-water

Table 1
Experimental conditions (median grain size diameter of Ottawa sand, d_{sand}; colloid diameter, $d_{colloid}$; volumetric water content, θ; Darcy flux, q) and the recovered fraction of colloids in the effluent (M_{eff}).

#	d_{sand} (μm)		$d_{colloid}$ (μm)	θ	q (cm/h)	M_{eff}
	Matrix	Lens				
1	710	360	3.2	0.320	7.56	0.607
2	710	360	1.0	0.323	7.26	0.613
3	710	240	3.2	0.320	6.12	0.505
4	710	240	1.0	0.328	6.54	0.614
5	710	150	3.2	0.339	7.74	0.536
6	710	150	1.0	0.329	7.62	0.636
7	360	710	3.2	0.318	7.2	0.297
8	360	710	1.0	0.309	5.7	0.585
9	240	710	3.2	0.321	6.48	0.221
10	240	710	1.0	0.307	7.02	0.532
11	150	710	3.2	0.328	6.90	0.148
12	150	710	1.0	0.329	6.36	0.435

velocity for the matrix and lens are respectively denoted by v_m and v_l while the volumetric water content of the matrix is denoted by θ_m — the water content for the lens θ_l follows from the total porosity. Fig. 7 shows the optimized and observed breakthrough curves. The bromide effluent curves were described fairly well judging by the r^2-values and the curves shown in Fig. 7. In the first six experiments the soil matrix is made up of the relatively permeable 710-μm Ottawa sand and transport occurs almost exclusively in the matrix. The results for the analytical model suggest that transport occurs in both lens and matrix for experiments 7 through 12, which is plausible because the 710-μm Ottawa sand is now the lens. The fit of the effluent data is slightly poorer and the breakthrough curves exhibited some tailing. The low values for the transfer coefficient α suggest limited transfer between the lens and the matrix for all twelve experiments. The difference in parameter values between a coarser matrix and a coarser lens (i.e., the 710-μm Ottawa sand) was further explored with a t-test for the mean. Table 3 shows the means for v_m, v_l, κ, and α as well the p values to assess significance in the difference between the means. For experiments 1 through 6 (coarser matrix) the pore-water velocity in the matrix of 24.5 cm/h far exceeds the mean velocity in the lens (v_l has a mean of 1.46 cm/h). On the other hand, the average velocity in the lens is 36.9 cm/h if it is made up of the coarser 710-μm Ottawa sand (experiments 7–12). The difference in velocity is highly significant both in

Table 2
Optimization to bromide breakthrough curves.

#	v_m (cm/h)	v_l (cm/h)	θ_m	κ (cm)	α (hr^{-1})	t_o (hr)	r^2
1	27.5	0	0.291	0.128	0.0972	1.30	0.9999
2	23.4	0.0191	0.289	0.0797	0.119	1.28	0.9996
3	21.3	8.76	0.296	0.138	0.015	1.29	1.0000
4	22.5	0	0.288	0.125	0.0894	1.29	0.9992
5	26.5	0	0.300	0.106	0.15	1.28	0.9995
6	26.0	0	0.295	0.133	0.0708	1.29	0.9995
7	15.8	40.9	0.201	0.443	0.0084	1.25	0.9989
8	11.8	30.0	0.180	0.209	0.231	1.24	0.9992
9	9.25	34.8	0.180	0.209	0.128	1.26	0.9987
10	10.1	37.3	0.165	0.241	0.123	1.26	0.9994
11	15.6	37.0	0.180	0.206	0.0246	1.25	0.9995
12	13.5	41.4	0.196	0.551	0	1.26	0.9990

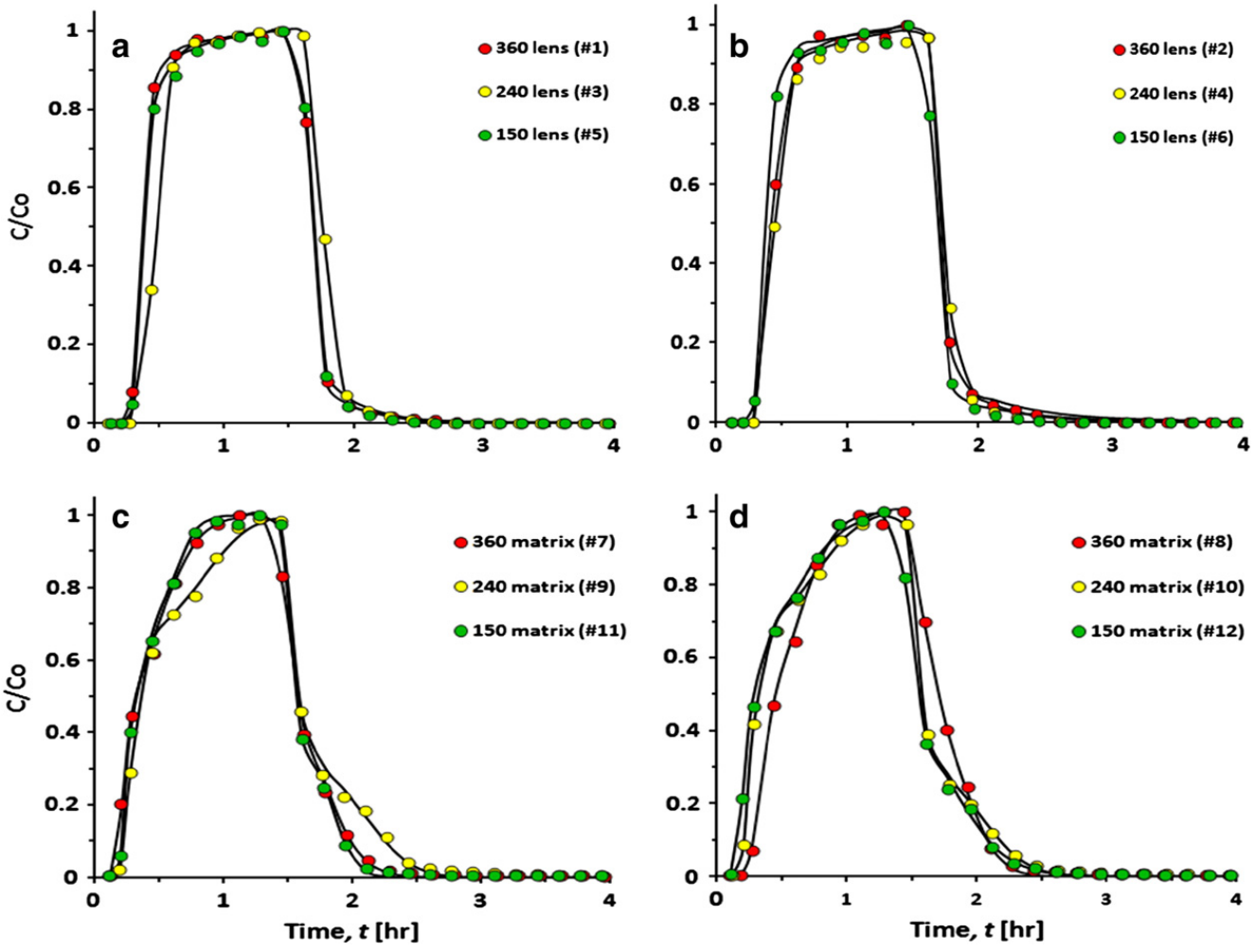

Fig. 7. Observed and optimized effluent curves for bromide tracer: a) 710-μm-Ottawa sand matrix and 3.2-μm colloid, b) 710-μm-Ottawa sand matrix and 1-μm colloid, c) 710-μm Ottawa sand lens and 3.2 μm colloid, and d) 710-μm Ottawa sand lens and 1-μm colloid.

the lens and the matrix. The mean dispersivity is 0.310 cm if there is appreciable flow in both lens and matrix (experiments 7–12) and a slight but significant reduction in κ occurs to a mean of 0.118 cm because almost all flow occurs in the matrix consisting of the 710-μm sand. There is no significant difference in the transfer parameter α between the coarse lens and matrix ($p = 0.922$).

4.3. Colloid effluent curves

Values for velocities and water contents that were optimized to the bromide data (Table 2) were also used to describe the colloid effluent curves. The optimization parameters were κ and α — bromide results will be different but were used as initial estimates nonetheless — and the retention parameters k_{am}, k_{sm}, k_{al}, k_{sl}, and k_d. Of course, it is desirable to lower the number of optimization parameters by conducting additional experiments to independently determine, for example, reaction parameters.

There is negligible flow in the fine-textured lens for experiments 1 through 6 (cf. Table 2). In this case the retention parameters for the lens were not optimized but set equal to those for the matrix instead. Optimized parameter values and the r^2-values are given for all twelve experiments in Table 4. A good description of the data was achieved with the exception of experiment 11. If the values in Table 4 are compared to those in Table 2, it appears that dispersivity has increased whereas there is less transfer between the two aqueous regions judging by the lower α. Fig. 8 depicts the effluent concentrations and the optimized breakthrough

Table 3
t-Test for difference between parameters for bromide transport in a medium with a 710-μm matrix or a 710-μm lens.

	#	v_m (cm/h)	v_l (cm/h)	κ (cm)	α (hr^{-1})
Mean 710-μm-matrix	1–6	24.5	1.46	0.118	0.0902
Mean 710-μm-lens	7–12	12.7	36.9	0.310	0.0858
p (two-tail)		6.64×10^{-8}	3.22×10^{-5}	0.0207	0.922

Table 4
Optimization to colloid effluent curves with the dual-permeability model.

#	κ (cm)	α (hr^{-1})	k_{am} (hr^{-1})	k_{sm} (hr^{-1})	k_{al} (hr^{-1})	k_{sl} (hr^{-1})	k_d (hr^{-1})	r^2
1	0.578	0.0004	1.447	0.365			0.119	0.9883
2	0.282	0.0374	0.105	0.953			0.221	0.9964
3	0.579	0	1.433	0.291			0.085	0.9908
4	0.264	0.0035	0.207	0.948			0.583	0.9978
5	0.559	0.0446	1.847	0			0.0648	0.9849
6	0.334	0.0249	0.193	0.934			0.321	0.9972
7	1.230	0.0001	6.478	0.0381	2.833	0.824	0.134	0.9862
8	0.402	0.0771	0.0882	0.550	0.0225	1.338	0.0513	0.9975
9	0.969	0	0.0713	7.324	2.939	3×10^{-4}	0.779	0.9555
10	0.581	0.0433	1.797	0	0	1.019	0	0.9985
11	2.599	0.0867	16.88	2.903	5.365	2.35	0.378	0.7794
12	1.158	0	2×10^{-4}	2.806	1.766	0.0624	0.0347	0.9978

curves. The effluent data were generally well described except for colloid concentrations near background levels ($C_e/C_o < 0.03$) such as in experiment 11.

Table 5 considers differences in parameter values due to colloid size or sand fraction. The first comparison is between the means of five optimized parameters for either a coarser matrix or lens. In experiments 1 through 6 the matrix was relatively coarse, with no independently optimized retention parameters for the lens, while in experiments 7 through 12 the lens was made up of the coarser 710-μm Ottawa sand.

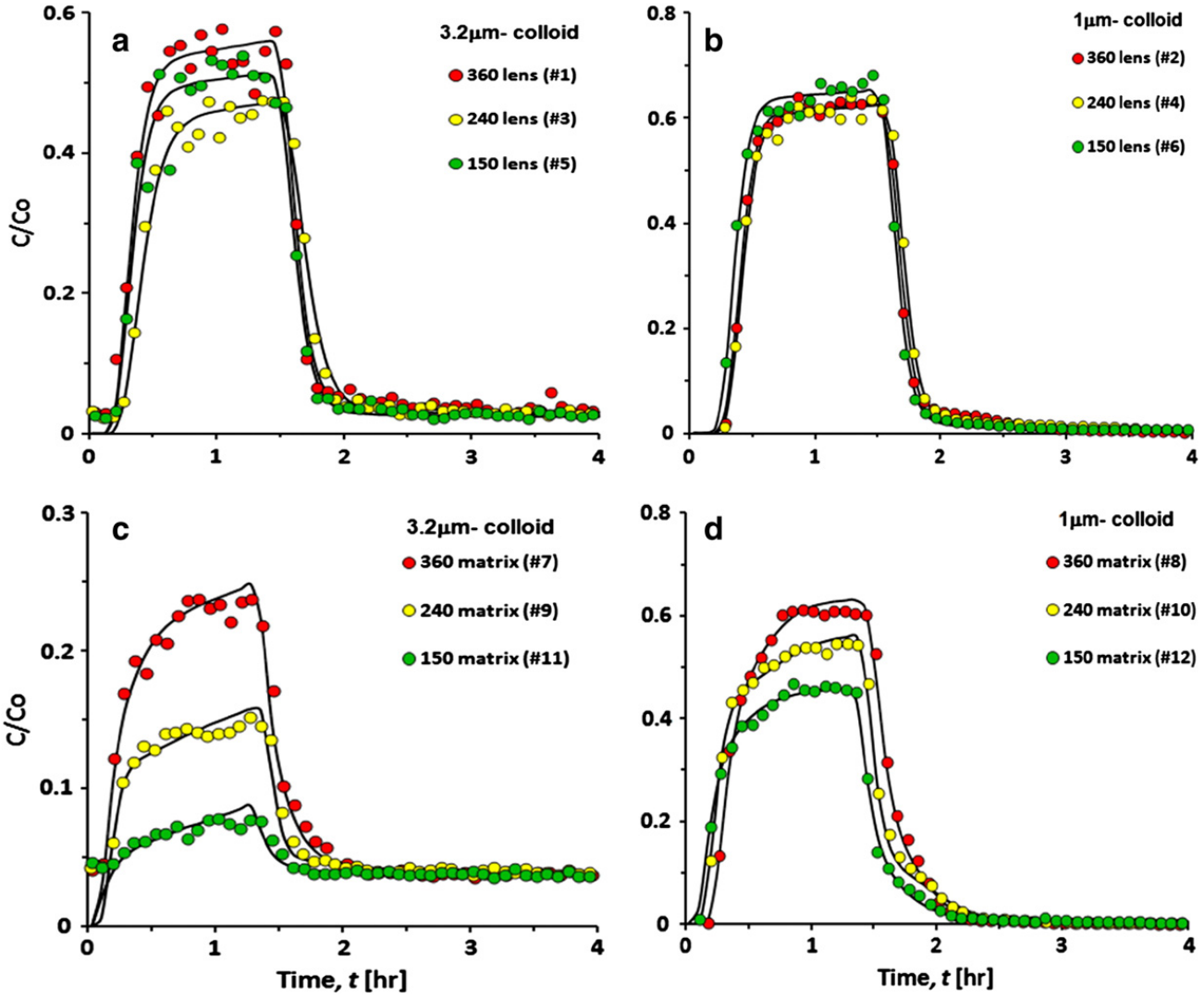

Fig. 8. Observed and optimized effluent curves for colloid particles: a) 710-μm-Ottawa sand matrix and 3.2-μm colloid, b) 710-μm-Ottawa sand matrix and 1-μm colloid, c) 710-μm Ottawa sand lens and 3.2 μm colloid, and d) 710-μm Ottawa sand lens and 1-μm.

Table 5
t-Test for difference between parameters of matrix and lens for colloid transport.

	#	κ (cm)	α (hr^{-1})	k_{am} (hr^{-1})	k_{sm} (hr^{-1})	k_{al} (hr^{-1})	k_{sl} (hr^{-1})	k_d (hr^{-1})
Mean 710-μm-matrix	1–6	0.433	0.0185	0.872	0.582			0.232
Mean 710-μm-lens	7–12	1.157	0.0345	4.219	2.270			0.230
p (two-tail)		0.0503	0.223	0.239	0.229			0.989
Mean 3.2-μm-colloid	1,3,5,7,9,11	1.086	0.0220	4.693	1.820	3.712	1.058	0.260
Mean 1.0-μm-colloid	2,4,6,8,10,12	0.504	0.0310	0.398	1.032	0.596	0.806	0.202
p (two-tail)		0.0295	0.716	0.177	0.575	6.09×10^{-3}	0.839	0.767

The dispersivity is greater for the coarser lens, when there is considerable flow in both matrix and lens, than in experiments 1 through 6 with the coarser matrix. The two-tail value for p is 0.0503, rendering the difference just insignificant at the 5% confidence level. All other differences between the mean are clearly not significant. Although not reported, there was also no significant difference in either reversible or irreversible retention between the mean for a 710-μm Ottawa sand, either lens or matrix, and that for the three other sands (150-, 240-, and 320-μm sands). The second comparison involves the means for the two different colloid sizes. The dispersivity is significantly ($p = 0.0295$) greater for the 3.2- than the 1-μm-colloids presumably because of greater tortuosity and fewer accessible pores for the larger colloid particles. All retentions rates appear greater for the larger 3.2-μm-colloids. This is in line with the breakthrough curves shown in Fig. 8 and the smaller fraction of the 3.2- than the 1-μm colloids that was recovered from the effluent (Table 1). However, a significant dependency of retention rate on colloid size could only be established for reversible retention in the lens material ($p = 6.09 \times 10^{-3}$). Although only three samples are compared, k_{al} is significantly greater for the larger colloids.

Finally, a comparison is made between the means of reversible and irreversible retention rates for both the coarser 710-μm-sand, either as lens or matrix, and the finer sands, only as matrix (Table 6). The first two rows of Table 6 pertain to both colloid sizes, subsequently only experiments with either 3.2- or 1-μm-colloids are considered. Except for the 1-μm-colloids, the rate of reversible retention is greater than that of irreversible attachment. The effect is only significant for retention of 3.2-μm colloids by the 710-μm sand ($p = 2.05 \times 10^{-3}$). Also notice that both reversible and irreversible rates appear greater for the finer than the coarse textured material for all colloid sizes. Perhaps due to the small sample size and the variability of the optimized parameters, this difference is not significant.

5. Summary and conclusions

An analytical solution was presented for reactive transport in a dual-permeability medium with reversible and irreversible mass transfer between the aqueous and the sorbed phases and linear exchange between the two aqueous phases. The solution was derived to provide an approximate description of subsurface colloid transport in aggregated media. The difference between flow rates in the two regions will affect the transport of the colloids. Furthermore, colloids are subject to complex attachment and straining processes that are controlled by a myriad of factors, among them the distinct hydrodynamics for the two flow domains. The analytical model can also be used to model transport of other reactive solutes in dual-permeability media. The solution for the concentrations in aqueous and solid phases were obtained using Laplace transformation and matrix decomposition as outlined in Appendix A.

The analytical solutions were used to illustrate the behavior of the (effluent) breakthrough curve for different values of the transfer parameter α (Fig. 3) and the dependency of depth profile on reversible and irreversible rates (Figs. 4 and 5). The analytical solution is convenient to partition the total concentration into two contributions from the aqueous phase and four from the solid phase.

Subsequently, the analytical model was used to describe effluent curves for a bromide tracer and 3.2- or 1-μm-colloids that were obtained by Bradford et al. (2004) for a composite medium made up of a cylindrical lens or core of sand and a surrounding matrix with sand of a different grain size. The analytical solution provided a very good description of the bromide tracer and yielded physically plausible estimates for the velocity in the two flow domains (Table 2). Subsequently, these velocities were used to describe breakthrough curves for the colloid particles. This involved optimization of dispersivity κ, transfer parameter α, and a maximum of five retention parameters. An adequate description of the data could be

Table 6
t-Test for difference in reversible and irreversible retention parameters for different sands.

	#	Colloid	k_a (hr^{-1})	k_s (hr^{-1})	p (two-tail)
Mean 710-μm-sand	1–12	1 and 3.2 μm	1.513	0.757	0.131
Mean 150-, 240-, or 360-μm-sand	7–12	1 and 3.2 μm	4.219	2.270	0.550
Mean 710-μm-sand	1,3,5,7,9, and 11	3.2 μm	2.644	0.638	2.05×10^{-3}
Mean 150-, 240-, or 360-μm-sand	7,9,11	3.2 μm	7.810	3.422	0.553
Mean 710-μm-sand	2,4,6,8,10, and 12	1 μm	0.382	0.876	0.321
Mean 150-, 240-, or 360-μm-sand	8, 10, 12	1 μm	0.628	1.119	0.748

achieved (Table 4). Dispersivity and retention parameters were typically greater for the larger 3.2-μm-colloids while both reversible and irreversible retention rates tended to be higher for the finer sands than the coarser 710-μm Ottawa sand. The relatively small sample size and the complex flow pattern in the composite medium made it difficult to reach definitive conclusions regarding transport parameters for colloid transport.

Appendix A. Solution procedure

The mathematical problem given by Eqs. (1)–(7) is solved by first taking the Laplace transform of the two governing equations, then decoupling and solving the resulting ordinary differential equations, and finally inverting to the regular time domain. The solution of a similar problem, albeit considerably simpler due to the omission of interaction with the solid phase, was treated in detail by Leij et al. (2012). In the following we will briefly review the solution procedure with an emphasis on novel aspects for the colloid transport model with attachment/detachment and irreversible retention.

The following Laplace transform with respect to time (with s as complex transformation variable)

$$L\{C_i(x,t)\} = \overline{C}_i(x,s) = \int_0^\infty C(x,t)\exp(-st)dt \tag{A1}$$

is applied to the governing Eq. (1), the boundary conditions (4)–(6), and the rate Eqs. (2) and (3). The resulting ordinary differential equation for transport in region i may be written as:

$$\kappa v_i \frac{d^2\overline{C}_i}{dx^2} - v_i\frac{d\overline{C}_i}{dx} = \left[s\left(1+\frac{k_{ai}}{s+k_d}\right)+k_{si}+\alpha_i\right]\overline{C}_i - \alpha_i\overline{C}_j \tag{A2}$$
$$(i=1,2; j=2,1)$$

where α_i is given by Eq. (15b).

The two governing equations are written in matrix form:

$$G(C) = AC \tag{A3}$$

with the advection–dispersion operator

$$G(..) = \kappa\frac{d^2..}{dx^2} - \frac{d..}{dx} \tag{A4}$$

while the coefficient matrix and solution vector are respectively given by:

$$\mathbf{A} = \begin{bmatrix} \frac{s}{v_1}\left(1+\frac{k_{a1}}{s+k_d}\right)+\frac{k_{s1}+\alpha_1}{v_1} & -\frac{\alpha_1}{v_1} \\ -\frac{\alpha_2}{v_2} & \frac{s}{v_2}\left(1+\frac{k_{a2}}{s+k_d}\right)+\frac{k_{s2}+\alpha_2}{v_2} \end{bmatrix}, \quad C = \begin{bmatrix} \overline{C}_1 \\ \overline{C}_2 \end{bmatrix}. \tag{A5a,b}$$

The system is diagonalizable by using the eigenvalues and eigenvectors of the coefficient matrix (Esfandiari, 2008; Kreyszig, 2006; Zwillinger, 1989). The resulting two ordinary differential equations are decoupled and can be readily solved to obtain the two respective concentrations in the Laplace domain. After implementing the boundary conditions, the solution for the first region is

$$\begin{aligned}\overline{C}_1(x,s) = \frac{C_o}{2}\exp\left(\frac{x}{2\kappa}\right)\Bigg\{&\left[\frac{a_1}{r}+\frac{1}{s}-\frac{1}{rs}\left(\frac{b_1}{s+k_d}-d_4\right)\right] \\ &\times\exp\left[-\frac{x}{\sqrt{2v_1v_2\kappa/a_2}}\sqrt{s-\left(\frac{b_2}{s+k_d}-d_2-\frac{v_1v_2}{2\kappa}-r\right)/a_2}\right] \\ &-\left[\frac{a_1}{r}-\frac{1}{s}-\frac{1}{rs}\left(\frac{b_1}{s+k_d}-d_4\right)\right] \\ &\times\exp\left[-\frac{x}{\sqrt{2v_1v_2\kappa/a_2}}\sqrt{s-\left(\frac{b_2}{s+k_d}-d_2-\frac{v_1v_2}{2\kappa}+r\right)/a_2}\right]\Bigg\}.\end{aligned} \tag{A6}$$

The variables a, b, c, and d were given by Eqs. (11a,b)–(14a,b) while the auxiliary variable r is defined by:

$$r = a_1\sqrt{\left(s-\frac{b_1/a_1}{s+k_d}+\frac{d_1}{a_1}\right)^2+\omega^2} \tag{A7}$$

with ω given by Eq. (15a,b). The inverse Laplace transform is carried out by using the shifting and convolution theorems.

The following transformation pairs are used that were obtained directly from Abramowitz and Stegun (1970) and Polyanin and Manzhirov (1998) or derived by using elementary properties of the Laplace transform:

$$L^{-1}\{\exp(-k\sqrt{s})\} = \frac{k}{\sqrt{4\pi t^3}}\exp\left(-\frac{k^2}{4t}\right) \tag{A8}$$

$$L^{-1}\left\{\frac{\exp\left(\pm k\sqrt{s^2+\omega^2}\right)}{\sqrt{s^2+\omega^2}}\right\} = H(t\pm k)J_0\left(\omega\sqrt{t^2-k^2}\right) \quad (k>0) \tag{A9}$$

$$L^{-1}\left\{\exp\left(\pm k\sqrt{s^2+\omega^2}\right)\right\} = \delta(t\pm k) - kJ_0\left(\omega\sqrt{t^2-k^2}\right) \pm \frac{\omega k H(t\pm k)}{\sqrt{t^2-k^2}}J_1\left(\omega\sqrt{t^2-k^2}\right) \quad (k>0) \tag{A10}$$

$$L^{-1}\left\{\exp\left(\frac{\omega}{s+k}\right)\right\} = \exp(-kt)\left[\delta(t)+\sqrt{\frac{\omega}{t}}I_1\left(2\sqrt{\omega t}\right)\right] \tag{A11}$$

$$L^{-1}\left\{\frac{1}{s}\exp\left(\frac{\omega}{s+k}\right)\right\} = \exp\left(\frac{\omega}{k}\right)J\left(\frac{\omega}{k},kt\right) \tag{A12}$$

$$L^{-1}\left\{\frac{1}{s(s+k)}\exp\left(\frac{\omega}{s+k}\right)\right\} = \frac{1}{k}\exp\left(\frac{\omega}{k}\right)\left[1-J\left(kt,\frac{\omega}{k}\right)\right] \tag{A13}$$

where H is the unit-step or Heaviside function, δ is the Dirac delta function, J_0 and J_1 are zero- and first-order Bessel functions of the first kind, I_0 and I_1 are the corresponding modified Bessel functions, and J denotes Goldstein's J-function (cf. Goldstein, 1953; van Genuchten, 1981). Substituting the expressions for the inverse Laplace transform in Eq. (A6) and evaluating the Dirac and Heaviside functions leads to the analytical solution given by Eqs. (8) and (9).

References

Abramowitz, M., Stegun, I.A., 1970. Handbook of Mathematical Functions. Dover Publications Inc., New York.

Beven, K., Germann, P., 1982. Macropores and water-flow in soils. Water Resources Research 18, 1311–1325.

Bradford, S.A., Torkzaban, S., 2008. Colloid transport and retention in unsaturated porous media: A review of interface-, collector-, and pore-scale processes and models. Vadose Zone Journal 7, 667–681.

Bradford, S.A., Simunek, J., Bettahar, M., van Genuchten, M.T., Yates, S.R., 2003. Modeling colloid attachment, straining, and exclusion in saturated porous media. Environmental Science & Technology 37, 2242–2250.

Bradford, S.A., Bettahar, M., Simunek, J., van Genuchten, M.Th., 2004. Straining and attachment of colloids in physically heterogeneous porous media. Vadose Zone Journal 3, 384–394.

Bradford, S.A., Simunek, J., Bettahar, M., Tadassa, Y.F., van Genuchten, M.T., Yates, S.R., 2005. Straining of colloids at textural interfaces. Water Resources Research 41, W10404.

Bradford, S.A., Torkzaban, S., Leij, F.J., Simunek, J., van Genuchten, M.T., 2009. Modeling the coupled effects of pore space geometry and velocity on colloid transport and retention. Water Resources Research 45, W02414.

Bradford, S.A., Torkzaban, S., Simunek, J., 2011. Modeling colloid transport and retention in saturated porous media under unfavorable attachment conditions. Water Resources Research 47, W10503.

Cey, E.E., Rudolph, D.L., 2009. Field study of macropore flow processes using tension infiltration of a dye tracer in partially saturated soils. Hydrological Processes 23, 1768–1779.

Cey, E.E., Rudolph, D.L., Passmore, J., 2009. Influence of macroporosity on preferential solute and colloid transport in unsaturated field soils. Journal of Contaminant Hydrology 107, 45–57.

Coats, K.H., Smith, B.D., 1964. Dead-end pore volume and dispersion in porous media. Society of Petroleum Engineers Journal 4, 73–84.

de Hoog, F.R., Knight, J.H., Stokes, A.N., 1982. An improved method for numerical inversion of Laplace transforms. SIAM Journal on Scientific and Statistical Computing 3, 357–366.

Dean, D.M., Foran, M.E., 1992. The effect of farm liquid waste application on tile drainage. Journal of Soil and Water Conservation 47, 368–369.

Dykhuizen, R.C., 1991. Asymptotic solutions for solute transport in dual-velocity media. Mathematical Geology 23 (3), 383–401.

Esfandiari, R.S., 2008. Applied Mathematics for Engineers. Atlantis Publishing Company, Los Angeles, CA.

Evans, M.R., Owens, J.D., 1972. Factors affecting the concentration of faecal bacteria in land-drainage water. Journal of General Microbiology 71, 477–485.

Gerke, H.H., van Genuchten, M.T., 1996. Macroscopic representation of structural geometry for simulating water and solute movement in dual-porosity media. Advances in Water Resources 19, 343–357.

Ginn, T.R., Wood, B.D., Nelson, K.E., Scheibe, T.D., Murphy, E.M., Clement, T.P., 2002. Processes in microbial transport in the natural subsurface. Advances in Water Resources 25, 1017–1042.

Goldstein, S., 1953. On the mathematics of exchange processes in fixed columns I: Mathematical solutions and asymptotic expansions. Proceedings of the Royal Society of London, Series A: Mathematical and Physical Sciences 219, 151–185.

Jarvis, N.J., 2007. A review of non-equilibrium water flow and solute transport in soil macropores: principles, controlling factors and consequences for water quality. European Journal of Soil Science 58, 523–546.

Javandel, I., Doughty, Ch., Tsang, C.-F., 1984. Groundwater Transport: Handbook of Mathematical Models. Water Resour. Monograph, no. 10. Am. Geophys. Union, Washington, D.C.

Kreyszig, E., 2006. Advanced Engineering Mathematics. John Wiley, New York.

Lapidus, L., Amundson, N.R., 1952. Mathematics of adsorption in beds.VI. The effects of longitudinal diffusion in ion exchange and chromatographic columns. Journal of Physical Chemistry 56, 984–988.

Leij, F.J., Bradford, S.A., 2009. Combined physical and chemical nonequilibrium transport model: analytical solution, moments, and application to colloids. Journal of Contaminant Hydrology 110, 87–99.

Leij, F.J., Toride, N., Field, M., Sciortino, A., 2012. Solute transport in dual-permeability porous media. Water Resources Research 48, W04523.

McGechan, M.B., Lewis, D.R., 2002. Transport of particulate and colloid-sorbed contaminants through soil, part 1: General principles. Biosystems Engineering 83, 255–273.

Pang, L., McLeod, M., Aislabie, J., Simunek, J., Close, M., Hector, R., 2008. Modeling transport of microbes in ten undisturbed soils under effluent irrigation. Vadose Zone Journal 7, 97–111.

Passmore, J.M., Rudolph, D.L., Mesquita, M.M.F., Cey, E.E., Emelko, M.B., 2010. The utility of microspheres as surrogates for the transport of *E. coli* RS2g in partially saturated agricultural soil. Water Research 44, 1235–1245.

Polyanin, A.D., Manzhirov, A.V., 1998. Handbook of Integral Equations. CRC Press, Boca Raton.

Ryan, J.N., Elimelech, M., 1996. Colloid mobilization and transport in groundwater. Colloids and Surfaces A: Physicochemical and Engineering Aspects 107, 1–56.

Selim, H.M., Ma, L., 1998. Physical Nonequilibrium in Soils: Modeling and Applications. Ann Arbor Press, Chelsea, MI.

Silliman, S.E., 1995. Particle transport through two-dimensional, saturated porous media: influence of physical structure of the medium. Journal of Hydrology 167, 79–98.

Simunek, J., van Genuchten, M.Th., 2008. Modeling nonequilibrium flow and transport processes using HYDRUS. Vadose Zone Journal 7, 782–797.

Simunek, J., He, C., Pang, L., Bradford, S.A., 2006. Colloid-facilitated solute transport in variably saturated porous media: numerical model and experimental verification. Vadose Zone Journal 5, 1035–1047.

Toride, N., Leij, F.J., van Genuchten, M.Th., 1993. A comprehensive set of analytical solutions for nonequilibrium solute transport with first-order decay and zero-order production. Water Resources Research 29, 2167–2182.

Toride, N., Leij, F.J., van Genuchten, M.Th, 1995. The CXTFIT code for estimating transport parameters from laboratory or field tracer experiments. Version 2.0. Res. Rep. 137. U.S. Salinity Lab, Riverside, CA.

Unc, A., Goss, M.J., 2003. Movement of faecal bacteria through the vadose zone. Water, Air, and Soil Pollution 149, 327–337.

van Genuchten, M.Th., 1981. Non-equilibrium transport parameters from miscible displacement experiments. Report 119. U.S. Salinity Laboratory, Riverside, CA.

van Genuchten, M.Th., Dalton, F., 1986. Models for simulating salt movement in aggregated field soils. Geoderma 38, 165–183.

van Genuchten, M.Th., Wierenga, P.J., 1976. Mass transfer studies in sorbing porous media: I. Analytical solutions. Soil Science Society of America Journal 40, 473–480.

Vanderborght, J., Kasteel, R., Herbst, M., Javaux, M., Thiéry, D., Vanclooster, M., Mouvet, C., Vereecken, H., 2005. A set of analytical benchmarks to test numerical models of flow and transport in soils. Vadose Zone Journal 4, 206–221.

Zwillinger, D., 1989. Handbook of Differential Equations. Academic Press, San Diego.